Journal of Quantitative Spectroscopy & Radiative Transfer 309 (2023) 108703

Contents lists available at ScienceDirect

Journal of Quantitative Spectroscopy & Radiative Transfer

journal homepage: www.elsevier.com/locate/jqsrt

High resolution FTIR spectrum of $CH_2D^{37}Cl$: ν_4 and ν_8 fundamental bands

Paolo Stoppa[a,*], Andrea Pietropolli Charmet[a], Filippo Tamassia[b], Elisabetta Canè[b], Mattia Melosso[c], Andrè Achilli[c], Luca Dore[c], Cristina Puzzarini[c]

[a] Dipartimento di Scienze Molecolari e Nanosistemi, Università Ca' Foscari Venezia, Via Torino 155, 30172 Mestre (VE), Italy
[b] Dipartimento di Chimica Industriale "Toso Montanari", Università di Bologna, Viale Risorgimento 4, 40136 Bologna, Italy
[c] Dipartimento di Chimica "Giacomo Ciamician", Università di Bologna, Via Selmi 2, 40126 Bologna, Italy

ARTICLE INFO

Article history:
Received 15 May 2023
Revised 13 June 2023
Accepted 13 June 2023
Available online 14 June 2023

Keywords:
Mono-deuterated chloromethane
Infrared spectrum
Spectroscopic parameters
Rovibrational analysis
Coriolis interactions

ABSTRACT

The high-resolution Fourier transform infrared spectrum of $CH_2D^{37}Cl$ has been analyzed in the region of the ν_4 and ν_8 bands from 1170 to 1370 cm^{-1}. The upper states of these fundamentals, separated by 0.6 cm^{-1}, interact with each other by *a*-type as well as *b*-type Coriolis resonance, and a strong asymmetric distribution of the intensity of the rotational structure in each band is observed. The spectral analysis resulted in the assignment of 2774 and 1611 rovibrational transitions for ν_4 and ν_8 bands, respectively, which have been simultaneously fitted using Watson's *A*-reduction Hamiltonian in the I^r representation and the relevant perturbation operators. A set of spectroscopic constants for the two fundamentals as well as seven coupling terms have been determined. From spectral simulations, the dipole moment ratio $|\Delta\mu_a/\Delta\mu_b|$ of ν_4 has been determined to be 1.3 ± 0.1 while the intensity ratio between ν_4 and ν_8 has been estimated to be 5.0 ± 1.0.

1. Introduction

Chloromethane (methyl chloride, CH_3Cl) is one of the most abundant chlorinated organic compounds in the Earth's atmosphere, with an average concentration of around 550 to 560 pptv observed in 2016 [1]. Its sources are either natural (plants, soils, algae, and bacteria in oceans) or anthropogenic (chemical activities, combustion of coal and biomass) [2]. Recently, both $CH_3{}^{35}Cl$ and $CH_3{}^{37}Cl$ isotopologues have been also detected in the gas surrounding the protostar IRAS 16,293–2422 and in the coma of comet 67P/Churyumov–Gerasimenko (67P/C-G) [3]. It is important to report that in the same protostar many deuterated molecules have been detected [4–9], thus pointing out that also CH_2DCl might be present. Indeed, despite the low cosmic abundance of deuterium with respect to hydrogen (*ca.* 1.6×10^{-5} part), deuterium atoms can be relatively abundant in interstellar molecules. This phenomenon is known as deuterium enrichment (or deuterium fractionation) and allowed the observation of many multiply-deuterated species with column densities comparable to those of the corresponding parent species [10].

Rotational and rovibrational spectroscopies are among the most widely applicable and accurate methods for remote sensing of trace gases, but to profit from their sensitivity, accurate spectroscopic parameters are required. For the parent molecule CH_3Cl numerous spectroscopic studies have been carried out, whereas for its deuterated forms only a few works are available in the literature. For this reason, we undertook the study of the mono-deuterate isotopic species (CH_2DCl). The low-resolution infrared spectrum of CH_2DCl has been analyzed by Riter and Egger in the 60 s [11], while only very recently a detailed study of the vibrational spectrum of this molecule has been performed up to 9000 cm^{-1} by Fourier transform infrared (FTIR) spectroscopy in conjunction with high-quality *ab-initio* calculations [12]. In the last years, some high-resolution infrared studies of $CH_2D^{35}Cl$ [13–15] and $CH_2D^{37}Cl$ [16] have been performed and accurate molecular parameters, including interaction constants, for different vibrational states have been obtained. The rotational spectra of mono-deuterated methyl chloride in the millimeter-wave region have been studied for the first time in 2020 [17] and subsequently, by extending the measurements up to 520 GHz, the set of the spectroscopic parameters of the ground vibrational state have been improved for $CH_2D^{35}Cl$ and $CH_2D^{37}Cl$ [12].

The present work deals with the analysis of the rovibrational structure of the ν_4 and ν_8 fundamental bands of $CH_2D^{37}Cl$ in the region around 8 μm, in which the high-resolution FTIR spectrum is

* Corresponding author.
E-mail address: stoppa@unive.it (P. Stoppa).

https://doi.org/10.1016/j.jqsrt.2023.108703
0022-4073/

Table 1
Observed avoided crossings between $\nu_4 = 1$ and $\nu_8 = 1$ states of $CH_2D^{37}Cl$ [a].

J	K_a ($\nu_4 = 1$)	K_a ($\nu_8 = 1$)
6 – 7	1^-	1^+
19 – 20	2^-	2^+
29 – 30	3^-	3^+
36 – 37	$4^\mp$	$4^\pm$
42 – 43	$5^\mp$	$5^\pm$

[a] The + and − upper signs refer to *even* ($K_a + K_c = J$) and *odd* ($K_a + K_c = J + 1$) levels, respectively.

investigated for the first time. The obtained results, together with the available data for the mono-deuterated chloromethane [12–17], constitute a base to assist and guide the search of this molecule in remote environments.

2. Experimental details

The $CH_2D^{37}Cl$ sample has been synthesized in our laboratory by reacting CH_2DOH (CDN Isotopes; 99.2% D-enriched) with $Na^{37}Cl$ (Cambridge Isotope Laboratory; 95% ^{37}Cl-enriched) and diluted sulphuric acid, following the procedure described for the ^{35}Cl isotopologue in Ref. [13].

The high-resolution (0.004 cm^{-1} unapodized) infrared absorption spectrum of $CH_2D^{37}Cl$ has been recorded at room temperature in the spectral region between 450 and 1600 cm^{-1} using a Bomem DA3.002 FTIR spectrometer [18,19] located at the University of Bologna (Italy). The sample has been kept at a pressure of 53 Pa in a multipass absorption cell with a total optical path length of 6 m. Eight hundred scans have been co-added to improve the signal-to-noise ratio of the spectrum and the line positions have been measured using the WSpectra software [20]. The absolute wavenumber scale of the spectrum has been calibrated against absorption lines of H_2O and CO_2 reported in the HITRAN database [21]. In the investigated range, the accuracy of the line positions is estimated 0.001 cm^{-1} for unblended lines and the measured full width at half maximum (FWHM) is about 0.0035 cm^{-1}.

3. Overview and description of the spectrum

$CH_2D^{37}Cl$ is a tetrahedral molecule belonging to the C_s symmetry point group; the symmetry plane contains the *a*- and *b*-axes, while the *c*-axis is perpendicular to it. This molecule is a nearly-prolate asymmetric-top rotor with Ray's asymmetry parameter $\kappa = -0.994$. The vibrational modes, all infrared active, are six of *A'* (ν_1 – ν_6) and three of *A"* (ν_7 – ν_9) symmetry species; the former give rise to *a*-/*b*-hybrid bands, while the latter produce *c*-type absorptions. The ν_4 (1268.20 cm^{-1}) and ν_8 (1267.62 cm^{-1}) vibrations are ascribed to the CH_2 wagging and C-D / CH_2 out-of-plane bending, respectively. The upper states of these fundamentals interact with each other by *a*-type as well as *b*-type Coriolis resonances. Since the interacting states are very close in energy, several avoided crossings due to *a*-type Coriolis resonance have been observed. The list of these crossings, shown in Table 1, coincides with that observed for $CH_2D^{35}Cl$ [15].

The intensity of the *p*-type ($\Delta K_a = -1$) and *r*-type ($\Delta K_a = +1$) sub-bands of ν_4 are depleted and enhanced, respectively, while for ν_8 the converse intensity perturbation is observed. This asymmetric distribution of the intensity of the rotational band structure, called negative perturbation [22], is due, in this case, to the negative sign of the *a*-type Coriolis ζ-constant. The comparison between the ${}^pP_3(J)$ and ${}^rR_1(J)$ lines strength of ν_4 and ν_8 is shown in Fig. 1; the intensity values have been calculated by the SPCAT program [23] with the constants obtained in the present work. In case of levels with avoided crossings, the intensity of the *p*- and *r*-type sub-bands is overturned at the crossing. As an example, in the *b1* and *b2* panels of Fig. 1 is shown the intensity of transitions with $K'_a = 2^-$ and 2^+ of ν_4 and ν_8, respectively, where the avoided crossing is observed at $J' = 19 - 20$. This effect arises from the different mixing between wavefunctions of the unperturbed rovibrational states $\nu_4 = 1$ and $\nu_8 = 1$ before and after the crossing points.

Although the strong Coriolis interaction alters the intensity of the absorptions and significantly shifts the lines near the avoided crossings, the *a*-type component structure of ν_4 is similar to that of a parallel band in prolate symmetric rotors. As an example, a portion of the *P* branch showing the displacement of the K_a features in the ${}^qP_K(7)$ and ${}^qP_K(8)$ clusters is depicted in Fig. 2. The effect of the *a*-type Coriolis coupling is evident in the significantly lower wavenumber shift for $K_a = 1^-$ of the ${}^qP_K(8)$ group. A section of the *Q* branch of the ν_4 fundamental in the range 1268 – 1270 cm^{-1} is shown in Fig. 3. The *Q* branch is formed by a series of ${}^qQ_K(J)$ clusters degrading towards higher wavenumbers for increasing K_a; within each multiplet, characterized by the first line with $J = K_a$, the *J* numbering increases towards lower wavenumbers, and the sequence is covered by the lines of the previous cluster. The *b*-type component of the ν_4 band extends over a wider spectral region than the *a*-type one and, as reported above, the *r*-type ($\Delta K_a = +1$) transitions appear more intense than the *p*-type ($\Delta K_a = -1$) ones. The *J* structure of the ${}^rQ_1(J)$ cluster is illustrated in Fig. 4, where the different degradation due to the asymmetry splitting is clearly visible; the spectral section also exhibits several transitions belonging to the stronger *a*-type component.

The ν_8 fundamental is a *c*-type band, and its intensity is comparable to the *b*-type component of ν_4. Due to negative perturbation, the *p*-type sub-bands are stronger than the *r*-type ones. A typical ${}^pQ_K(J)$ multiplet is illustrated in Fig. 5, the degradation to lower wavenumber as *J* increases is clearly visible. Due to the *a*-type Coriolis interaction with ν_4, an additional *pseudo a*-type component of ν_8 with selection rules $\Delta J = 0, \pm1$, $\Delta K_a = 0, \pm2, \ldots$ and $\Delta K_c = 0, \pm2, \ldots$ has been identified. As an example, two consecutive ${}^qQ_K(J)$ multiplets of this weak special component are shown in Fig. 6.

4. Results and discussion

The analysis of the experimental data began with calculating the ν_4 and ν_8 rovibrational transitions; this has been done using Watson's *A*-reduced Hamiltonian up to the sixth order in the I^r representation [24] and the perturbation operators for the *a*- and *b*-type Coriolis resonances. For the ground state, the constants reported in Ref. [12] have been employed, while for the upper states, preliminary values of the vibrational energy, rotational constants, and Coriolis ζ-terms obtained from *ab-initio* calculation have been used [12]. The predictions of transitions and data fitting have been carried out using the Visual SPCAT and Visual SPFIT programs [25], respectively, which are based on Pickett's CALPGM program suite [23]. The assignment of the spectral transitions has been performed with the support of the Loomis-Wood type diagram as implemented in the Visual Loomis-Wood software [25].

The assignment began from the strongest ${}^qP_K(J)$ and ${}^qR_K(J)$ lines of ν_4 with $K_a \leq 3$ and $J' \leq 25$ far from the avoided crossings, and some $K'_a = 0$ lines of ν_8. The identified transitions have been used to refine upper state constants together with the band origins and Coriolis interaction parameters. The analysis proceeded iteratively with the identification of new lines of both bands with higher quantum numbers and the revision of constants. Already for $K'_a > 3$ transitions, the inclusion of the *a*- and *b*-type Coriolis terms depending on *J* and *K* ($\xi^{a,J}_{4,8}$, $\xi^{a,K}_{4,8}$, $\xi^{b,J}_{4,8}$, $\xi^{b,K}_{4,8}$) has been necessary to reduce the fit standard deviation to an acceptable value, and to obtain parameters of the excited states that did not differ too much

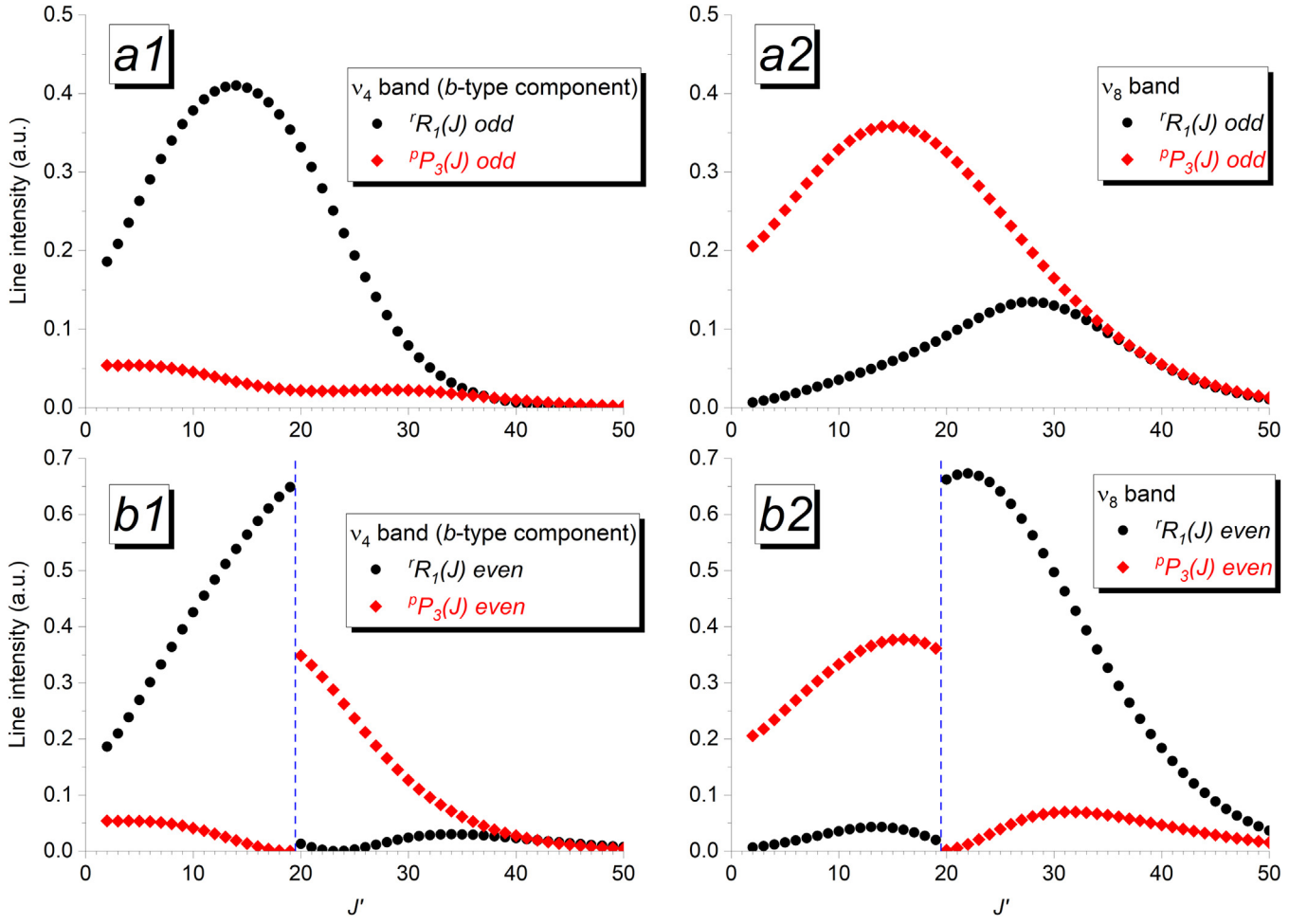

Fig. 1. Comparison between ${}^{p}P_3(J)$ and ${}^{r}R_1(J)$ lines strength of the ν_4 and ν_8 band calculated by the constants of Table 3. *Even* and *odd* refer to $(K_a'' + K_c'' = J'')$ and $(K_a'' + K_c'' = J'' + 1)$ transitions, respectively. In the *b1* and *b2* panels, the vertical dash line indicates the J' position of the avoided crossing between the $K_a = 2$ *odd* and $K_a = 2$ *even* levels of $\nu_4 = 1$ and $\nu_8 = 1$, respectively.

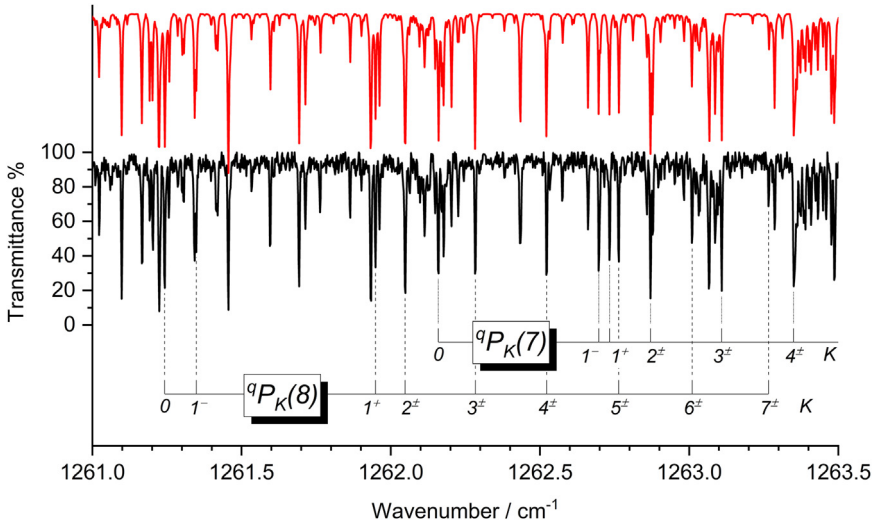

Fig. 2. Details of the K_a structure of two consecutive ${}^{q}P_K(J)$ multiplets of the ν_4 *a*-type component; the + and − − signs refer to *even* $(K_a'' + K_c'' = J'')$ and *odd* $(K_a'' + K_c'' = J'' + 1)$ levels, respectively, while the ± sign refers to the unsplitted ones. It is worth noting the strong shift of the ${}^{q}P_{K=1}(8)$ line due to *a*-type Coriolis coupling. Upper trace: simulated spectrum, lower trace: experimental spectrum.

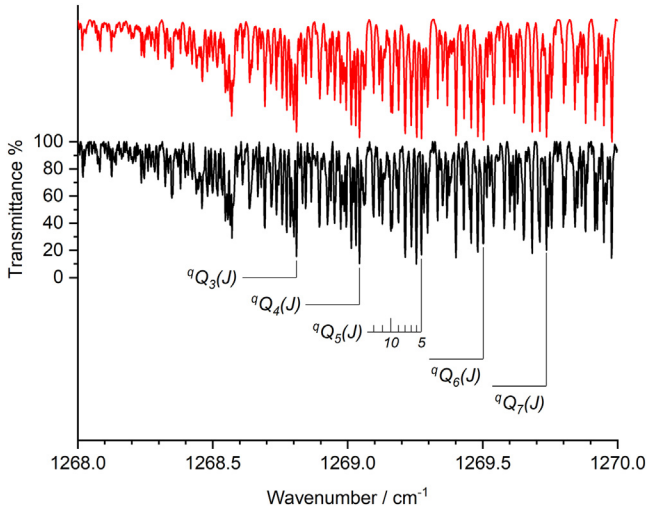

Fig. 3. Spectral portion of the *a*-type *Q*-branch of the ν_4 band of $CH_2D^{37}Cl$ where some lines of the $^qQ_5(J)$ manifold are indicated. Upper trace: simulated spectrum, lower trace: experimental spectrum.

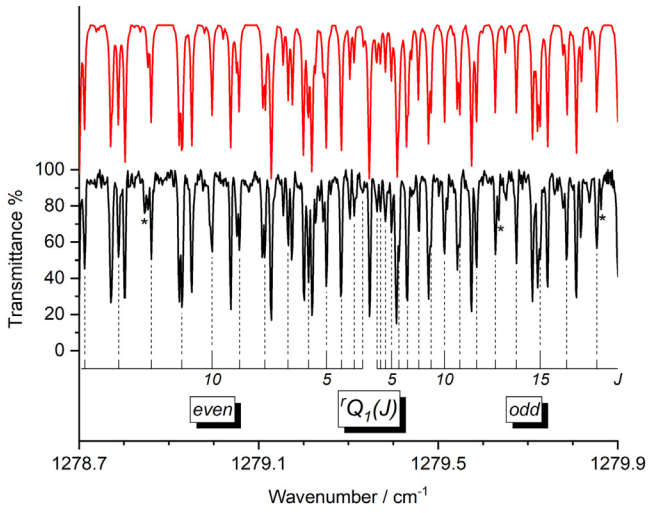

Fig. 4. Details of the fine structure of the $^rQ_1(J)$ cluster of the ν_4 *b*-type component of $CH_2D^{37}Cl$ showing the asymmetry splitting in the *even* ($K_a" + K_c" = J"$) and *odd* ($K_a" + K_c" = J" + 1$) transitions. Features marked by asterisk belong to $CH_2D^{35}Cl$. Upper trace: simulated spectrum, lower trace: experimental spectrum.

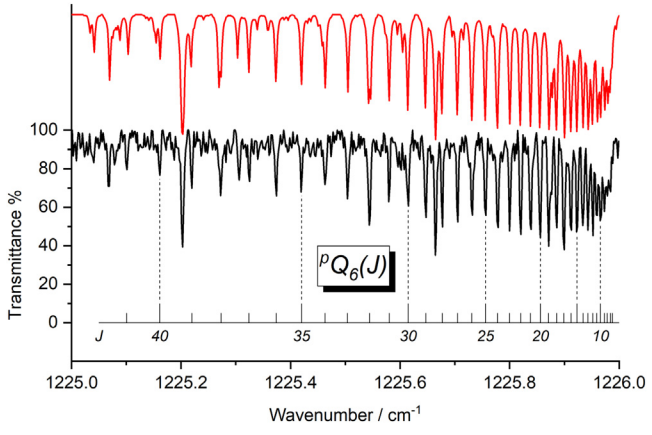

Fig. 5. Spectral portion of the *P*-branch of ν_8 fundamental of $CH_2D^{37}Cl$. Upper trace: simulated spectrum. Lower trace: experimental spectrum showing the *J* structure of the $^pQ_6(J)$ manifold; the additional observed features are $^qP_K(J)$ and $^pP_K(J)$ lines belonging to ν_4 and ν_8, respectively.

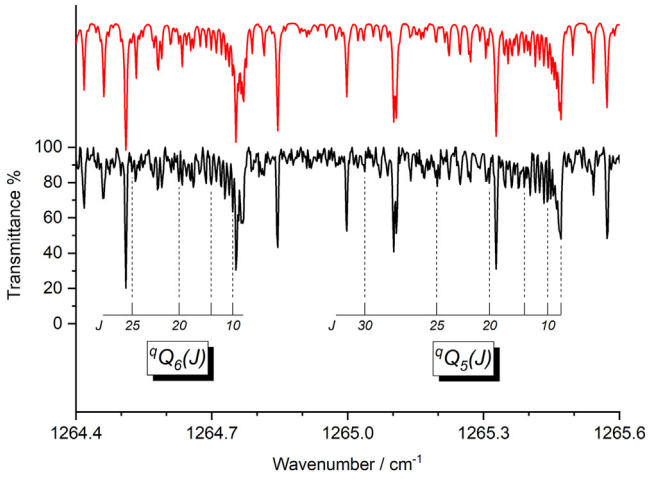

Fig. 6. Portion of the $CH_2D^{37}Cl$ spectrum showing the *J* structure of the $^qQ_5(J)$ and $^qQ_6(J)$ manifolds of the *pseudo-a*-type component of the ν_8 band. The strongest unlabeled lines are due to ν_4 $^qP_K(J)$ transitions. Upper trace: simulated spectrum, lower trace: experimental spectrum.

from the ground-state counterparts. Once a substantial number of lines of ν_4 and ν_8 have been assigned, further improvement of the fit has been obtained by considering the high-order *b*-type Coriolis resonance coefficient $\theta^b_{4,8}$. The matrix elements of the perturbation operators employed in the present analysis are reported in Table 2.

The molecular constants obtained from the best fit are collected in Table 3, which also includes the ground state constants and some details on the lines fitted. For the latter, it is interesting to note that because of the negative perturbation, the assigned lines of ν_4 with $\Delta K_a = +1$ are many more than those with $\Delta K_a = -1$ (1125 *vs* 124), and the opposite happens for the ν_8 band (72 *vs* 896). Furthermore, it should be noted that the 643 transitions of ν_8 with $\Delta K_a = 0$ all belong to the *pseudo*-parallel component. The standard deviation of the fit is 0.631×10^{-3} cm^{-1}, which means well within the estimated accuracy of the measurements, and all fitted transitions shows deviations (in absolute value) lower than 0.003 cm^{-1}. The refined parameters appear well statistically determined. The rotational constants are close to those of the ground state, the differences being within 0.8% except for the *A* constant of $\nu_8 = 1$ for which the percentage rises to 1.5%. However, the value of this parameter, as well as the other rotational constants of the upper states, are very similar to those obtained through *ab-initio* calculations [12] as it can been seen in Table 4, where the experimental *vs* calculated Coriolis parameters are also reported. Concerning the centrifugal distortion constants, the larger deviations with respect to the ground state occurs for the Δ_{JK} (35%) and Δ_{JK} (34%) parameters of $\nu_4 = 1$, and $\nu_8 = 1$, respectively. As it can be seen, the differences are of similar magnitude but opposite sign, so the average value of Δ_{JK} of the two upper states approaches to the value of the ground state. This is commonly observed when strong interactions are present [26], and, in this case, it is due to the strong correlation between this constant and some interactions terms ($\xi^{b,J}_{4,8}$, $\xi^{b,K}_{4,8}$, $\theta^b_{4,8}$).

The values of the δ_K distortion term, the sextic centrifugal distortion coefficients of the upper states, and the δ_J parameter of $\nu_8 = 1$ have been constrained to that of the ground state because, if these parameters are allowed to vary in the fit, indeterminate values or values markedly different from those of the ground state are obtained. This can be explained by the fact that the values of these parameters are very small and transitions with higher *J* and K_a quantum numbers are necessary for their satisfactory determination.

Table 2
Matrix elements of the perturbation operators considered in the analysis.

a-type Coriolis: $\langle v_4 = 1, J, K\|\boldsymbol{H}^a\|v_8 = 1, J, K\rangle = [\xi^a_{4,8} + \xi^{a,J}_{4,8}J(J+1) + \xi^{a,K}_{4,8}K^2]K$
b-type Coriolis: $\langle v_4 = 1, J, K\|\boldsymbol{H}^b\|v_8 = 1, J, K \pm 1\rangle = (i/2)[\xi^b_{4,8} + \xi^{b,J}_{4,8}J(J+1) + \xi^{b,K}_{4,8}K^2]F(J,K)$
b-type Coriolis: $\langle v_4 = 1, J, K\|\boldsymbol{H}^b\|v_8 = 1, J, K \pm 3\rangle = (i/8)\theta^b_{4,8}\ F(J,K)F(J,K \pm 1)F(J,K \pm 2)$
$F(J,K) = \sqrt{J(J+1) - K(K \pm 1)}$
$\xi^a_{4,8} = A_e\zeta^a_{4,8}(\omega_4 + \omega_8)/\sqrt{\omega_4\omega_8}$
$\xi^b_{4,8} = B_e\zeta^b_{4,8}(\omega_4 + \omega_8)/\sqrt{\omega_4\omega_8}$

Table 3
Spectroscopic parameters (cm^{-1}) of the $v_4 = 1$ and $v_8 = 1$ states of $CH_2D^{37}Cl$ [a].

	Ground State [b]	$v_4 = 1$	$v_8 = 1$
E		1268.199070(90)	1267.619301(123)
A	3.99726227	4.015209(35)	3.936406(35)
B	0.4095536976	0.40922829(67)	0.40884453(52)
C	0.3997920842	0.39660712(74)	0.40008061(65)
Δ_J x 10^6	0.48641	0.44588(26)	0.51203(35)
Δ_{JK} x 10^5	0.5070745	0.68305(105)	0.33173(127)
Δ_K x 10^4	0.55202	0.61685(84)	0.43844(110)
δ_J x 10^7	0.116744	0.1162(21)	0. 116,744 [c]
δ_K x 10^6	0.7825	0.7825 [c]	0. 7825 [c]
	Φ_J x $10^{12} = -0.142$, Φ_{JK} x $10^{10} = 0.101$, Φ_{KJ} x $10^9 = 0.11819$, Φ_K x $10^8 = 0.256$		
	ϕ_J x $10^{13} = 0.102$, ϕ_{JK} x $10^{12} = 0.394$, ϕ_K x $10^9 = 0.357$ [d]		
	$\xi^a_{4,8} = -0.301522(35)$, $\xi^{a,J}_{4,8}$ x $10^5 = -0.5980(82)$, $\xi^{a,K}_{4,8}$ x $10^3 = 0.7116(47)$,		
	$\xi^b_{4,8} = 0.2223658(137)$, $\xi^{b,J}_{4,8}$ x $10^6 = -0.597(20)$, $\xi^{b,K}_{4,8}$ x $10^2 = -0.2275(20)$,		
	$\theta^b_{4,8}$ x $10^5 = -0.20821(143)$		
No. of lines		2774	1611
σ x 10^3 (cm^{-1})		0.631	
Range of J'		0 – 48	1 – 40
Range of K'_a		0 – 13	0 – 10
No. of lines with $\Delta K_a = -1$		124	896
No. of lines with $\Delta K_a = 0$		1525	643
No. of lines with $\Delta K_a = +1$		1125	72

[a] Quoted uncertainties are one standard deviation in units of the last significant digits.
[b] From Ref. [12].
[c] Fixed to the ground state value.
[d] Ground state sextic centrifugal distortion constants [12], fixed for the upper levels.

Table 4
Experimental and calculated values (cm^{-1}) of the rotational constants and Coriolis terms of the $v_4 = 1$ and $v_8 = 1$ states of $CH_2D^{37}Cl$.

Vibrational state	Parameter	Obs.[a]	Calc.[b]	Diff.%[c]
$v_4 = 1$	A	4.015209	4.010005	0.13
	B	0.4092283	0.4090460	0.04
	C	0.3966071	0.3968496	0.06
$v_8 = 1$	A	3.936406	3.9464836	0.26
	B	0.4088445	0.4090426	0.05
	C	0.4000806	0.4001374	0.01
	$\lvert\xi^a_{4,8}\rvert$	0.30152	0.31550	4.64
	$\lvert\xi^b_{4,8}\rvert$	0.22237	0.23026	3.55

[a] Present work.
[b] From Ref. 12.
[c] Diff.% is the percentage of the difference between Observed and Calculated values.

The comparison of the present results with those of the corresponding analysis for the $CH_2D^{35}Cl$ [15] point out that the asymmetric distribution of the rotational structure intensity for ν_4 and that for ν_8 are similar, and the observed position of the avoided crossings is the same. Furthermore, the data set, the fitted rovibrational and interaction parameters are similar; the main discrepancy is in the opposite sign of the a-type Coriolis term. In the present work we have considered both signs for the Coriolis terms: the agreement between the observed and calculated spectra is obtained only when $\xi^a_{4,8}$ and $\xi^b_{4,8}$ have negative and positive signs, respectively.

To test the reliability of the obtained parameters, to calculate the transition dipole moment ratio along the a and b axes in ν_4, and the band intensity ratio between ν_4 and ν_8, many simulations of different spectral portions have been performed. A Lorentzian line profile with a FWHM of 0.0035 cm^{-1} at the temperature of 298 K has been adopted in such spectral simulations. The best match to the observed intensities in the ν_4 band has been obtained for $|\Delta\mu_a/\Delta\mu_b| = 1.3 \pm 0.1$ while the intensity ratio between ν_4 and ν_8 has been estimated to be 5.0 ± 1.0, which is in good agreement with the *ab-initio* computed value of 4.9 [12]. The spectra calculated in different spectral regions of ν_4 and ν_8 for $CH_2D^{37}Cl$ show a good agreement with the experimental spectrum as shown in the upper trace of Figs. 2–6 and in Fig. 7 where the overview of the spectrum in the 1200 – 1340 cm^{-1} region and the simulation of the ν_4 / ν_8 band system is shown.

We have also considered the possible interactions of $v_4 = 1$ and $v_8 = 1$ states with the next closer $v_3 = 1$ (1435 cm^{-1}) and $v_6 = 2$ (1410 cm^{-1}) levels. From symmetry consideration, a- and b-type Coriolis resonance can occur between $v_8 = 1/v_3 = 1$ and $v_8 = 1/v_6 = 2$, while c-type Coriolis interaction as well as anharmonic resonance may take place between $v_4 = 1/v_3 = 1$ and $v_4 = 1/v_6 = 2$. Calculations of the rovibrational energy levels predict some avoided crossings for $K_a \geq 6$ levels of the $v_4 = 1$ and $v_8 = 1$ states due to high-order Coriolis and anharmonic resonances, but no irregularities have been observed in the spectrum. Furthermore, several fits have been performed including the interactions with the $v_3 = 1$ and $v_6 = 2$ states but no improvement. Therefore, it can be assumed that the fitted transitions are not significantly perturbed by the $v_3 = 1$ and $v_6 = 2$ states.

A complete list of all fitted transitions is deposited as supplementary material.

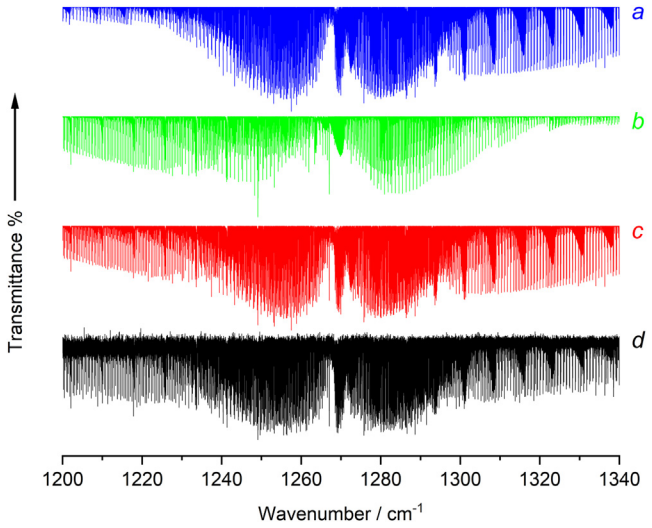

Fig. 7. Survey FTIR spectrum of the ν_4 and ν_8 bands of $CH_2D^{37}Cl$. Traces (a) and (b) refer to the simulation of the ν_4 and ν_8 bands, respectively; trace (c) is their sum, and trace (d) is the observed spectrum.

5. Conclusions

A detailed rovibrational study of the nearly degenerate ν_4 and ν_8 bands of $CH_2D^{37}Cl$ in the 1170 – 1370 cm^{-1} region has been performed for the first time. The upper states of these fundamentals interact via *a*- and *b*-type Coriolis resonances; several avoided crossings have been observed and a *pseudo-a*-type component of the ν_8 has been identified.

The spectral analysis resulted in the identification of 2774 and 1611 rovibrational transitions for the ν_4 and ν_8, respectively, and in the determination of accurate coupling constants and spectroscopic parameters in the *A*-reduction scheme. The reliability of the results achieved is confirmed by the good agreement between calculated and observed spectra. Moreover, the spectral simulations led to the determination of the intensity ratio of the ν_4 and ν_8 bands, and the transition dipole moment ratio for the *a*- and *b*-type components of ν_4. For both bands, the analysis of the asymmetric distribution of the rotational structure intensity due to the perturbations allowed us to determine the negative sign of the *a*-type Coriolis ζ-constant.

The possible interactions of the $\nu_4 = 1$ and $\nu_8 = 1$ states with the next closer $\nu_3 = 1$ and $\nu_6 = 2$ levels have also been considered, but no evidence has been observed for the assigned transitions.

The results of this investigation can be useful for supporting and guiding the detection of $CH_2D^{37}Cl$ in astronomical spectra and for the refinement of the potential function of chloromethane.

Declaration of Competing Interest

The authors declare that they have no known competing financial interests or personal relationships that could have appeared to influence the work reported in this paper.

CRediT authorship contribution statement

Paolo Stoppa: Conceptualization, Validation, Formal analysis, Investigation, Data curation, Writing – original draft, Writing – review & editing, Visualization, Supervision, Project administration. **Andrea Pietropolli Charmet:** Investigation, Validation, Resources, Writing – review & editing. **Filippo Tamassia:** Investigation, Validation, Writing – review & editing. **Elisabetta Canè:** Writing – review & editing. **Mattia Melosso:** Validation, Writing – review & editing, Visualization. **Andrè Achilli:** Formal analysis, Investigation. **Luca Dore:** Writing – review & editing. **Cristina Puzzarini:** Writing – review & editing, Funding acquisition.

Acknowledgements

We gratefully acknowledge the financial support by University Ca' Foscari Venezia (ADiR funds) and by Bologna University (RFO funds). This work has also been supported by MUR (PRIN Grant Number 202082CE3T). The authors also gratefully remember Mr. A. Baldan for the synthesis of the CH_2DCl sample.

Supplementary materials

Supplementary material associated with this article can be found, in the online version, at doi:10.1016/j.jqsrt.2023.108703.

References

[1] Engel A, Rigby M, Burkholder JB, Fernandez RP, Froidevaux L, Hall BD, Hossaini R, Saito T, Vollmer MK, Yao B. Update on ozone-depleting substances (ODS) and other gases of interest to the Montreal Protocol. Scientific assessment of ozone depletion: 2018, Geneva, Switzerland: World Meteorological Organization; 2018. ch.1.

[2] Keppler F, Röhling AN, Jaeger N, Schroll M, Hartmann SC, Greule M. Sources and sinks of chloromethane in a salt marsh ecosystem: constraints from concentration and stable isotope measurements of laboratory incubation experiments. Environ Sci Proc Impacts 2020;22:627–41.

[3] Fayolle EC, Öberg KI, Jørgensen JK, Altwegg K, Calcutt H, Müller HSP, Rubin M, van der Wiel MHD, Bjerkeli P, Bourke TL, et al. Protostellar and cometary detections of organohalogens. Nat Astron 2017;1:703–8.

[4] Coutens A, Vastel C, Caux E, Ceccarelli C, Bottinelli S, Wiesenfeld L, et al. A study of deuterated water in thelow-mass protostar IRAS 16293-2422. Astron Astrophys 2012;539 Article A132.

[5] Melosso M, Bizzocchi L, Sipilä O, Giuliano BM, Dore L, Tamassia F, Martin–Drumel M-A, Pirali O, Redaelli E, Caselli P. First detection of NHD and ND_2 in the interstellar medium: amidogen deuteration in IRAS 16293-2422. Astron Astrophys 2020;641 Article A153.

[6] Bacmann A, Faure A, Hily-Blant P, Kobayashi K, Ozeki H, Yamamoto S, Pagani L, Lique F. Deuterium fractionation of nitrogen hydrides: detections of NHD and ND_2. Mon Notices Royal Astron Soc 2020;499:1795–804.

[7] Müller HSP, Jørgensen JK, Guillemin J-C, Lewen F, Schlemmer S. Rotational spectroscopy of mono-deuterated oxirane (*c*-C_2H_3DO) and its detection towards IRAS 16293−2422 B. Mon Notices Royal Astron Soc 2023;518:185–93.

[8] Müller HSP, Jørgensen JK, Guillemin J-C, Lewen F, Schlemmer S. Rotational spectroscopy of oxirane-*2,2-d*$_2$, *c*-CD_2CH_2O, and its tentative detection toward IRAS 16293-2422 B. J Mol Spectrosc 2023;394 Article 111777.

[9] Richard C, Jørgensen JK, Margulès L, Motiyenko RA, Guillemin J-C, Groner P. Torsional-rotational spectrum of doubly deuterated dimethyl ether (CH_3OCHD_2). Astron Astrophys 2021;651 Article A120.

[10] Ceccarelli C, Caselli P, Bockelee-Morvan D, Mousis O, Pizzarello S, Robert F, Semenov D. Deuterium Fractionation: the Ariadne's Thread from the Pre-collapse Phase to Meteorites and Comets today. In: Beuther H, Klessen R, Dullemond C, editors. Protostars and planetsvi. Tucson: University of Arizona Press; 2014. p. 859–82. Th. Henning, editors. Protostars and Planets VI.

[11] Riter JR, Eggers DF. Fundamental vibrations and force constants in the partially deuterated methyl halides. J Chem Phys 1966;44:745–58.

[12] Pietropolli Charmet A, Stoppa P, De Lorenzi A, Melosso M, Achilli A, Dore L, Puzzarini C, Canè E, Tamassia F. Computational, rotational, and rovibrational experimental investigation of monodeuterated chloromethane. J Quant Spectrosc Radiat Transf 2023;305 Article 108624.

[13] Baldacci A, Stoppa P, Pietropolli Charmet A, Giorgianni S, Nivellini G. High resolution FTIR study of the ν_5 and ν_6 bands of $CH_2D^{35}Cl$: analysis of resonances and determination of ground and upper state constants. Mol Phys 2005;103:2803–11.

[14] Baldacci A, Visinoni R, Giorgianni S, Nivellini G. High-resolution FTIR spectroscopy of $CH_2D^{35}Cl$: rovibrational analysis of the ν_3, ν_9 fundamentals and the $2\nu_6 - \nu_6$, $\nu_5 + \nu_6 - \nu_6$ hot bands. Mol Phys 2008;106:1233–40.

[15] Baldacci A, Visinoni R, Nivellini G. High-resolution FTIR spectroscopy of $CH_2D^{35}Cl$: analysis of the nearly degenerate ν_4 and ν_8 levels. Mol Phys 2010;108:2395–410.

[16] Stoppa P, Pietropolli Charmet A, De Lorenzi A, Tamassia F, Melosso M, Canè E, Dore L, Puzzarini C. High resolution FTIR study of the ν_5, ν_6, and ν_9 fundamental bands of $CH_2D^{37}Cl$. J Quant Spectrosc Radiat Transf 2021;270 Article 107719.

[17] Melosso M, Achilli A, Tamassia F, Canè E, Pietropolli Charmet A, Stoppa P, Dore L. High-resolution millimeter-wave spectroscopy of CH_2DCl: paving the way for future astronomical observations of chloromethane isotopologues. J Quant Spectrosc Radiat Transf 2020;248 Article 106982.

[18] Bizzocchi L, Tamassia F, Laas J, Giuliano BM, Degli Esposti C, Dore L, Melosso M, et al. Rotational and high-resolution infrared spectrum of HC_3N:

global ro-vibrational analysis and improved line catalog for astrophysical observations. Astrophys J Suppl Ser 2017;233 Article 11. doi:10.3847/1538-4365/aa9571.

[19] Tamassia F, Melosso M, Dore L, Pettini M, Canè E, Stoppa P, Pietropolli Charmet A. Spectroscopy of a low global warming power refrigerant. Infrared and millimeter-wave spectra of trifluoroethene (HFO-1123) in the ground and some vibrational excited states. J Quant Spectrosc Radiat Transf 2020;248 Article 106980.

[20] Carleer MR. WSpectra: a Windows program to accurately measure the line intensities of high-resolution Fourier transform spectra, in Remote Sensing of Clouds and the Atmosphere V. J.E. Russel, K. Schäfer, O. Lado-Bordowsky, editors. Proc SPIE-Int Soc Opt Eng 2001;4168:337–42.

[21] Gordon IE, Rothman LS, Hargreaves RJ, Hashemi R, Karlovets EV, Skinner FM, et al. The HITRAN2020 molecular spectroscopic database. J Quant Spectrosc Radiat Transf 2022;277 Article 107949.

[22] Mills IM. Coriolis interactions, intensity perturbations and potential functions in polyatomic molecules. Pure Appl Chem 1965;11:325–44.

[23] Pickett HM. The fitting and prediction of vibration-rotation spectra with spin interactions. J Mol Spectrosc 1991;148:371–7.

[24] Watson JKG. Vibrational spectra and structure, Vol. 6, New York/Amsterdam: Elsevier; 1977. Ed. J. R. Durig.

[25] Tasinato N, Pietropolli Charmet A, Stoppa P. ATIRS package: a program suite for the rovibrational analysis of infrared spectra of asymmetric top molecules. J Mol Spectrosc 2007;243:148–54.

[26] Bane MK, Thompson CD, Robertson EG, Appadoo DRT, McNaughton D. High-resolution FTIR spectroscopy of the ν_8 and Coriolis perturbation allowed ν_{12} bands of ketenimine. Phys Chem Chem Phys 2011;134:6793–8.